Outbursts from a Black Hole via Alfvén Wave to EM Wave Mode Conversions

James Daniel and Toshiki Tajima
Department of Physics and Institute for Fusion Studies
The University of Texas at Austin
Austin, Texas 78712 USA

ABSTRACT

A new mechanism for outbursts from a black hole is proposed. A recent work on general relativistic plasma equilibria around a black hole has shown the possibility of equilibrium presence of matter and magnetic fields in the neighborhood of the event horizon even where the corpuscular equilibrium is not allowed ($r < 3R_s$, where R_s is the Schwarzschild radius). A large amplitude Alfvén pulse in the black hole electron-positron atmosphere that propagates away from the hole into lower magnetic field regions can experience resonance and mode-convert itself into a large amplitude electromagnetic (EM) pulse. It is shown theoretically and computationally that through this process a large amount of mass can be picked up by the solitary EM pulse capable of traveling in vacuum, with which particles are accelerated to relativistic energies. Photon spectra are obtained not inconsistent with observation, which follow a multiple power law with log-log slopes of approximately -1, before a "knee" in the spectrum at energies slightly greater than 1 MeV. It is suggested that this may be a possible mechanism for the outbursts of the black hole binary GRO J1655-40.

1. Introduction

Black holes have long been suspected of generating outbursts, including γ-ray bursts, via a variety of mechanisms (Tanaka 1989; Murakami 1988). A blackhole has some properties, especially with respect to possible instabilities, that can generate bursts. In particular, a prime black hole candidate, GRO J1655-40, has demonstrated bursty optical properties that may indicate an advection-dominated accretion flow for the inner regions of the accretion disk (Orosz et al, 1997), and is generally believed to be a black hole binary. As such, it is motivation to investigate the near-black-hole plasma physics and its role in generating bursts. A framework of fully general relativistic plasma physics in both a cosmological metric (Holcomb and Tajima 1989) and the Schwarzschild metric (Tarkenton 1996; Buzzi et al, 1995) has provided some progress, and a more detailed study is now possible. Based on such a development, Tarkenton (1996) has investigated theory of general relativistic plasma equilibria with or without magnetic fields around a Schwarzschild black hole.

A corpuscular body whose equilibria are determined by the black hole gravity and the centrifugal force does not have a stable equilibrium orbit for the radius within $3R_s$, where R_s is the Schwarzschild radius (Misner, Thorne, and Wheeler 1973). The gas (or plasma) dynamics is different from the above corpuscular dynamics, where the fluid is under the gaseous (or plasma) pressure (i.e. collisions-mediated force) influence in addition to the above forces. It has been demonstrated, in face, that there exist equilibria of plasma (with or without magnetic field) around the event horizon (Tarkenton 1996). At this moment we do not know the stability of these equilibria. In fact, since matter is differentially rotating in most of these equilibira, it is likely that many of these equilibria suffer instabilities from shearing flows, just as matter in an accretion disk does through the magnetic shearing instability (Balbus & Hawley 1991). Instabilities may be also generated from the accretion

of disk matter into the region within $3R_s$. When such an instability sets in, perturbations of vortices (clumps) grow. Different from the accretion disk matter, matter within $3R_s$ upon such clump formation suffers the corpuscular instability. The corpuscular instability and a rapid infall of matter within $3R_s$ can cause bending of the equilibrium magnetic field, which triggers an intense magnetic pulse. This is equivalent to a (subcyclic or solitary) large amplitude shear Alfvén wave. Furthermore, non-general relativistic work with PIC simulations in a highly stratified positron-electron atmosphere near a neutron star demonstrate a possibility of particle (electron and positron) acceleration via Alfvén waves (Holcomb and Tajima 1992). A variation of this method was briefly demonstrated in a recent paper (Daniel and Tajima 1997), employing the physics of interaction between a subcyclic pulse and a plasma (Rau, Tajima, and Hojo 1996), and is explored more fully here.

In section II, we briefly review the formalism and theory behind our fully general relativistic Schwarzschild plasma, as well as means of linearly analysing resonance, cutoff and mode conversion. Section III shows linear and nonlinear simulations, the latter generating both particle acceleration and apparent solitons. Possible means of particle acceleration are also discussed. Section IV discusses the observable photon spectra generated by the simulations of electron acceleration in III, and Section V contains discussion and summary.

2. Formalism

2.1. Conformalism approach

We have taken the 3+1 formalism of Thorne and MacDonald (MacDonald and Thorne 1982; Thorne et al 1986) and employ a conformalism of the metric and physical quantities such that the equations become "flat": no covariant derivatives are involved in

the equations, and the general relativistic effects are hidden only in the change of plasma variables. Details of this formalism are can be found in (Daniel and Tajima 1997). The conformalized variables are $\vec{E}_\xi = \alpha\vec{E}$, $\vec{B}_\xi = \alpha\vec{B}$, $n_\xi = \alpha^2 n$, and $\vec{J}_\xi = \alpha^2\vec{J}$, where ξ is the conformalized spatial coordinate:

$$\xi(r) = (r - R_s) + R_s\, ln(r - R_s) + \text{const}, \tag{1}$$

$\alpha(r) = \sqrt{1 - \frac{R_s}{r}}$ is the lapse function, and n is the local number density of all species taken together. This spatial coordinate has been used previously for dealing with wave equations in the Schwarzschild metric (Futterman et al 1988). The constant is chosen to be zero for our simulations. The ξ spatial coordinate has the property that velocities measured in this framework are identical to locally measured velocities. The conformalism only considers propagation in the $\pm\vec{r}$ direction, and employs a 'slab' metric (we choose a particular $\vec{r}$ with $\theta = \theta_0$, $\phi = \phi_0$ and treat it as cartesian coordinates), $ds^2 = \alpha^{-2}\, dr^2 + dy^2 + dz^2$ $(= \alpha^2\, d\xi^2 + dy^2 + dz^2)$, which prevents spherically symmetric artifacts. This is useful if we consider the (point-like) wave source is away from the origin (as a matter of fact, it is close but outside of the horizon). In general, all the results to be considered will be discussed solely in conformalized coordinates and parameters (ξ-space), and graphed in these coordinates. While it is possible to show results in the non-conformalized (r-space) coordinates, they are not as informative in this format, and the graphs would be unreadable: in r-space the ξ grid is compressed on the left side, with several hundred cells within $r < 100$, and the amplitude of the E and B fields scales as α^{-1}, so that the amplitudes near $r = R_s$ are orders of magnitude higher than those far from the event horizon. Another reason for showing results in ξ-space rather than r-space is that several properties of plasma physics can be readily employed in ξ-space, such as dispersion relations, resonant and cutoff behavior, and mode conversion from one type of wave to another.

One concern of using the conformalized set of equations is keeping track of how they

relate to the real physics that might be observed far from the hole. As $r \to \infty$, $\alpha \to 1$, so the local physics far from the hole is "flat", and the time far from the hole is universal time. The conformalized ξ-space physics is the same far from the hole as the local physics far from the hole. If we model, for example, some phenomena occurring near the hole from which is emitted some observable electromagnetic wave that propagates far from the hole, the frequency in the model is the same as that which would be observed. The main concern is dealing with the proper time, τ, of the phenomenon near the hole, where the effects of time dilation are significant. Since $d\tau = \alpha dt$, then $\omega_\tau = \alpha^{-1}\omega_t$, where ω_τ is the locally measured frequency, and ω_t is the frequency measured in ξ-space as well as the frequency measured far from the hole. The proper time becomes important when there are physically known frequencies, such as that of electron-positron annihilation, that must be translated into universal time.

2.2. Electron-Positron Dispersion Relation

The plasma variables such as the plasma frequency and cyclotron frequency can vary as a function of ξ though the lapse function as the main result of our conformalism, even for a plasma which is uniform in the physical (r) coordinate:

$$\omega_p = \sqrt{\frac{4\pi\alpha^2(r(\xi))n_e(r(\xi))e^2}{m}} \tag{2}$$

$$\Omega_e = \frac{e\alpha(r(\xi))B_0(r(\xi))}{mc}. \tag{3}$$

High frequency electromagnetic waves in a nonuniform plasma (i.e., ξ-dependent ω_p and Ω_e) can be characterized by a local dispersion relation in the WKB sense. We will be considering linearly polarized transverse EM waves in an electron-positron plasma. We assume the proton density negligibly small compared with those of electrons and

positrons. The wave vector is chosen to be $\vec{k} = k\,\hat{\xi}$ and the background magnetic field is $\vec{B}_0 = B_0\,cos\,\theta\,\hat{\xi} + B_0\,sin\,\theta\,\hat{z}$, where θ is the angle between the $\vec{B}_0$ and $\vec{k}$. The main benefit of the conformalism is that now the dispersion relation for this plasma looks completely "flat" and only general relativistic effects appear through the modification of plasma parameters through Eqs. (2) and (3). It is given locally in ξ-space as (for perpendicular polarization: $\vec{E}_1 = E_1\hat{y}$, $\vec{B}_1 = B_1\hat{z}$)

$$\eta^2 \equiv \frac{c^2k^2}{\omega^2} \equiv \epsilon(k,\omega) = 1 - \frac{2{\omega_p}^2}{\omega^2}\left(1 - \frac{\Omega_e^2 cos^2\theta}{\omega^2} - \frac{\Omega_e^2 sin^2\theta}{\omega^2 - {c_s}^2k^2}\right)^{-1}, \tag{4}$$

and by (for parallel polarization: $\vec{E}_1 = E_1\hat{z}$, $\vec{B}_1 = B_1\hat{y}$)

$$\eta^2 = 1 - \frac{2{\omega_p}^2}{\omega^2}\left(1 - \frac{\Omega_e^2 cos^2\theta}{\omega^2}\right)^{-1}, \tag{5}$$

where η is the index of refraction, $\epsilon(k,\omega)$ is the dielectric function for transverse electromagnetic waves, Ω_e is the local electron cyclotron frequency, and ω_p is the local electron plasma frequency defined in Eqs. (2) and (3). By choosing special particular values for θ we can simplify the above equations for $\vec{B}_0 \| \vec{k}$ ($\theta = 0$):

$$\omega^2 - c^2k^2 = 2\omega_p^2\left(1 - \frac{\Omega_e^2}{\omega^2}\right)^{-1}, \tag{6}$$

and for $\vec{B}_0 \perp \vec{k}$ ($\theta = \pi/2$) with E_y, B_z polarity

$$\omega^2 - c^2k^2 = 2\omega_p^2\left(1 - \frac{\Omega_e^2}{\omega^2 - {c_s}^2k^2}\right)^{-1}, \tag{7}$$

and with E_z, B_y polarity

$$\omega^2 - c^2k^2 = 2\omega_p^2. \tag{8}$$

We will exclusively concern ourselves with the dispersion described by case Eq. (6) (E_y, B_z polarity, though the polarities are symmetric for $\theta = 0$).

2.3. Mode Conversion

One of the important consequences of the dispersion relation obtained in Sec. 2.2 for general relativistic plasma in the conformalism is that the radial (ξ) variation of the metric and other background parameters comes through only ω_p and Ω_e and thus one can turn the analysis of the effects of the metric into wave dynamics in a nonuniform background. That is, the plasma frequency varies both as a function of background density and the lapse function α, and the cyclotron frequency similarly varies as a function of both background magnetic field and the lapse function. Given these background profiles and an initial wave frequency and location, a WKB analysis reveals where in ξ-space resonance or cutoff behavior will occur ($\eta^2(\omega)$ goes to infinity at a resonance, and to zero at a cutoff). There are only two primary modes for transverse EM waves in an electron-positron plasma with $\vec{B}\|\vec{k}$: a shear Alfvén mode, which only exists for frequencies less than Ω_e (the resonance frequency for this mode) and cannot exist in vacuum, and an EM mode which is capable of propagating in vacuum, but does not exist for frequencies less than $\sqrt{2\omega_p^2+\Omega_e^2}$ (the cutoff frequency for this mode). It is possible for a wave of one mode to reach a point in ξ-space where a cutoff (or resonance) is reached, and evanesce through a region in which the mode is evanescent ($k^2<0$) to a resonance (or cutoff) that is not far from the first critical point. Upon reaching the far side of the resonance/cutoff pair (also known as a "Budden turning point" (Budden 1961)), the original wave has excited a new mode, which will propagate normally. If the cutoff of a Budden turning point is reached first (EM mode to Alfvén mode conversion) some of the wave will reflect, some will be transmitted, and some will be absorbed. If the resonant point is reached first (Alfvén to EM mode conversion), there is no reflection, some energy is absorbed, and the rest is transmitted. The WKB wave equation at a Budden turning point is

$$\Psi'' + k^2(\xi,\omega)\Psi = 0 \tag{9}$$

and $k^2(\xi,\omega)$ can be approximated as

$$k^2(\xi) = \frac{\beta}{\xi} + \frac{\beta^2}{\chi^2} \tag{10}$$

where $\frac{\beta^2}{\chi^2} = k_\infty^2$, $\chi = |\Delta\xi k_\infty|$, $\Delta\xi$ is the distance between the resonance and the cutoff of the turning point, k_∞ is the wavenumber far from the turning point, and ω is the particular frequency of the mode (treated as a constant in this case). For mode conversion to occur, $\chi = |\Delta\xi k_\infty|$ should not be much greater than unity. When χ is much greater than unity, the Budden turning point acts as a near-perfect wave absorbing point for Alfvén waves, an important property of the Budden turning point.

The local dispersion relation strongly affects the likelihood of mode conversion. In an overdense plasma, the two branches are far from each other: Fig. (1a) shows such a dispersion relation for $\omega_p = 1.0$ and $\Omega_e = 0.5$ as measured in code units (frequency in the code is measured vs an average plasma frequency which is normalized to $\overline{\omega_p} = 1$, where the overline indicates the average over the space of this nonuniform plasma, and without the overline indicates the local quantity, time is measured in units of the inverse plasma frequency $\overline{\omega_p}^{-1} = 1$, and other normalizations will be explained in Section III where we introduce the code). Fig. (1b) shows the relation for $\omega_p = 0.5\overline{\omega_p}$ and $\Omega_e = 0.25\overline{\omega_p}$. For a wave of frequency $\omega = 0.35\ \overline{\omega_p}$ (a typical frequency employed in our simulations), the wave can exist in the first dispersion relation as an Alfvén wave, but it is evanescent in the second. In order to have $|\Delta\xi k_\infty|$ be of order one or less for an overdense ($\frac{\omega_p}{\Omega_e} > 1$) plasma, the local number density must change radically over a very short distance. In an underdense ($\frac{\omega_p}{\Omega_e} < 1$) plasma, the possibility of mode conversion is much more likely, especially if $\omega_p \ll \Omega_e$, so that the resonant and cutoff frequencies are nearly equal. Fig. (2) shows how close the two branches get for the case of $\omega_p = \frac{\Omega_e}{16}$. Fig. (2a) shows frequency $\omega = 0.35$ in the Alfvén mode and Fig. (2b) shows the same frequency in the EM mode. The difference between the two modes is small, so $|\Delta\xi k_\infty|$ can be small without an extraordinarily large

change in the number density over distance. In weakly magnetized plasmas, therefore, we can expect little or no mode conversion to take place, but a strongly magnetized plasma can have efficient mode conversion from Alfvén to EM modes (and vice versa) because the evanescent region will always be small.

3. Linear and Nonlinear Wave Dynamics

3.1. PIC code

We developed a $1\frac{2}{2}$ particle-in-cell (PIC) code (Tajima 1989) appropriate for simulating self-consistently electromagnetic plasma phenomena near the event horizon and have discussed it previously (Daniel and Tajima 1997). In Tajima (1989), a general discussion on PIC code in a general metric is given. We also employ the absorbing boundary conditions at either end of the box (Tajima and Lee 1981). The PIC code is used instead of a fluid code to study the high-frequency phenomena in a plasma, and most especially to be able to model particle acceleration, which would be precluded in a fluid model.

That the code is $1\frac{2}{2}$ dimensional means that quantities can be functions of only one spatial parameter. There is only the one spatial degree of freedom in which particles and waves can propagate. It also means that the electromagnetic field vectors can exist in any direction, and that the momentum of the particles can exist in any direction (i.e., particles are said to be planar). Typical runs are done with about 20,000 particles, half electrons and half positrons, in 2048, 4096 or 8192 cells in the one-dimensional grid, and the size of a cell is about two thirds of a particle size. The grid spacing corresponds directly to ξ-space, and the code's fields, density, and momenta are the conformalized quantities, not necessarily the local quantities. The electron plasma frequency is defined as one, and time is measured in inverse plasma frequencies. The time step is typically 0.1 $\overline{\omega_p}^{-1}$, where $\overline{\omega_p}$ is the average

(in ξ-space) plasma frequency. We will be graphing spatially-dependent parameters vs. ξ, which is the grid spacing of the cells. Refer to Eq. (1) to recall the relation between the distance to the event horizon and ξ. The numerical value assigned to the Schwarzschild radius is $R_s = 220$ (in a unit of the grid size Δ_ξ). The background density is chosen to vary as $n(r) \propto e^{-\frac{r-R_s}{h}}$ and the background magnetic field varies as $\vec{B}_0(r) \propto e^{-\frac{r-R_s}{2h}}$ where h is an arbitrary scale height. Fig. (3) shows the typical conformalized background plasma frequency (based on the conformalized density) and background cyclotron frequency (based on the conformalized magnetic field. In the particular cases considered, $R_s = 220\ \Delta_\xi$ and $h = 150\ \Delta_\xi$ (for ξ far from the event horizon). These values are chosen such that the phenomena to be observed fits within the framework of the code, and do not readily translate to astronomical scales. The wave pulses we will be modelling will originate around $\xi = 416$ (about 40 units from the event horizon, as measured in r-space), near the peak conformalized density and magnetic field

There are four major sets of results to be presented here: (i) a demonstration of mode conversion for the linear case (small amplitude) initial wave, (ii) a simulation of particle trapping and acceleration by a short, high-amplitude sinusoidal pulse and by a high-amplitude subcyclic pulse, (iii) an analysis of possible means of particle acceleration, (iv) an analysis of the apparent soliton formation from particles ejected from the black hole atmosphere.

3.2. Linear Mode Conversion Simulation

We have previously demonstrated mode conversion behavior in a black hole atmosphere (Daniel and Tajima, 1997). Here, we revisit our previous results and demonstrate the validity of the linear Budden turning point approximation. Fig. (4) shows the index of

refraction as a function of ξ: in the background we have chosen, there is a Budden turning point at about $\xi \approx 1020$. The function $k^2(\xi)$ can be analyzed with Eqs. (9) and (10). There is no reflection coeffiecient (the wave reaches resonance first), and there is a transmission coefficent of

$$|T| = e^{-\frac{1}{2}\pi\chi} \tag{11}$$

where $|T|$ is the absolute value of the amplitude (not the square of the amplitude) and χ is as was defined for Eq. (10). In this case, the distance between resonance and cutoff is $\Delta\xi \approx 30$ and $k_\infty \approx .0879$ in code units, which implies a transmission coefficient of $|T| \approx 0.0159$. By measuring the ratio $\frac{|E_y|}{|B_z|} = \frac{\omega}{kc} = \frac{1}{n} = \frac{v_{ph}}{c}$ for the pulse as it propagates, we can determine whether the pulse is in the Alfvén or EM branch.

Fig. (5) shows the result of a simulation with $|E_y(t=0)| = 0.005$ in code units (i.e., $\frac{eE}{m_e\overline{\omega_p}^2\Delta_\xi} = 0.005$, where Δ_ξ is the grid size, and similarly for the magnetic field), which should demontrate the linear behavior predicted by the Budden analysis. Fig (5a) shows the initial pulse caught at the resonance point ($\xi = 1020$), with $|B_z| \gg |E_y|$. The amplitude has already attenuated significantly, and the wave energy will eventually be completely absorbed here. Some of the wave is transmitted, as predicted by the Budden analysis, and is shown in Fig. (5b). Its amplitude is very low, only about twice that of the background oscillations, but the longer wavelength reveals that it is the transmitted portion of the wave. Also, $E_y = B_z$ everywhere for this graph, so all this field energy is propagating to the right of the graph at the speed of light in the EM mode, as opposed to the previous graph's obvious Alfvén mode, so mode conversion has occurred. The amplitude can only very roughly be measured, but $|E_y| \approx 0.0001$ which means that the measured transmission is $|T| \approx 0.02$, which agrees very closely with the predicted value.

3.3. Nonlinear Mode Conversion

With a much higher amplitude ($|E_y(t=0)| = 2.5$ in code units), the linear results do not hold true any more. Fig. (6) shows the simultaneous E_y, B_z and n vs ξ at two successive times. At $t = 200.0\ \overline{\omega_p}^{-1}$, the wave is past the resonance predicted at $\xi = 1020$. Furthermore, the amplitude is still about $|E_y| \approx 1.0$, which implies that the transmission coefficient previously calculated does not apply in the nonlinear case. From an observational standpoint, this is useful information. Linearly, only about 1% of the wave amplitude gets through, and that is 0.01% of the initial wave energy. In this case, however, a significant 40% of the wave amplitude is transmitted, which improves the likelihood of detection for a distant observer. Another property of the emitted wave is that it carries a significant portion of particles (labeled as n in Fig. (6)), and the phase space graphed in Fig. (7) indicates that the particles are traveling with the wave. At $t = 300.0\ \overline{\omega_p}^{-1}$, the wave has carried the particles well beyond the resonance point at $\xi = 1020$. The mode of the wave is indeterminate, however. There is a precursor ($1500 < \xi < 1650$) in Fig. (6b), which is definitely in the EM mode ($E_y = B_y$), but the main part of the wave has the property that $\frac{v_{ph}}{c} = \frac{E_y}{B_z} < 1$, which is nominally the Alfvén mode.

Note that the Alfvén mode properties are existing well beyond the turning point ($1200 < \xi < 1500$), partly due to the locally high density which is orders of magnitude higher than the background density. A phenomenon we may call as self-induced transmission has occurred. [An optical parallel, self-induced transparency, has been discovered by (McCall and Hahn, 1969).] That is, the highly nonlinear nature of the wave has captured many particles, allowing the wave to continue self-consistently in the Alfvén mode, as if it had never "seen" the Budden turning point. Its phase velocity is approximately $\frac{v_{ph}}{c} = \frac{E_y}{B_z} \approx 0.8c$, which means that particles can conceivably travel along with it, which would not be the

case if it converted to EM mode, with $v_{ph} \geq c$.

We can determine where the majority of the acceleration takes place in this simulation. At $t = 200.0\ \overline{\omega_p}^{-1}$, the maximum value of $\gamma\beta$ ($= \frac{p_\xi}{mc}$, i.e. γ is the Lorentz factor and $\gamma^2 = (1-\beta^2)^{-1}$) is up to about 4.2 in Fig. (7). At $t = 300.0\ \overline{\omega_p}^{-1}$, the value has increased to 5.1, not significantly higher than before (when velocities were already relativistic. Most of the acceleration occurred between $t = 100.0\overline{\omega_p}^{-1}$ and $t = 200.0\overline{\omega_p}^{-1}$: Figure (8) is a parametric plot of $\gamma\beta_{max}$ ($= \frac{p_x}{mc}$) vs ξ, at even ($25.0\ \overline{\omega_p}^{-1}$) time intervals. The momentum increases geometrically in the Alfvén region ($\xi < 1020$), but the acceleration slows down after the mode conversion ($\xi > 1050$) into the EM branch. At around $\xi \approx 1200$, the acceleration picks up again, and continues until it reaches a maximum value far from the hole.

3.4. Bursty Acceleration out of a Black Hole Atmosphere

Particle acceleration possibly triggered from a violent motion of matter near the event horizon may be simulated with this computational model. We have done this previously (Daniel and Tajima 1997), but now we analyze our results in more detail. We can imagine a situation where accreting matter (Blaes 1987) interacts with the magnetic field of the blackhole magnetosphere (Mobarry and Lovelace 1986) and this accreting mass motion can trigger Alfvén wave pulse(s). This situation is a bit similar to that considered for (compressional) Alfvén wave acceleration around a neutron star (Holcomb and Tajima 1992). The initial setup is similar to the mode conversion discussed in the previous subsection. In fact, the initial amplitude we employ is the same as that of the previous case. The main difference is that the Alfvén pulse is a solitary wave, with a $sech^2(\xi - v_{gr}t)$ profile. (It is imperfectly generated, so part of the initial pulse travels toward the horizon

on the left side of the grid, and bounces off the reflective boundary condition there, which also decreases the initial amplitude of the right-propagating wave. This is because the frequency of this "wave" is broad banded and instantaneous wave turn-on is difficult. The physics of interest is elsewhere on the grid, and the secondary pulse does not change the qualitative results.) Fig. (9) shows the index of refraction for the wide range of frequencies of this pulse. As the figure shows, resonance will occur for the various frequencies over a range of $\xi \approx 1150$ to $\xi \approx 1175$, with the lower bands of frequencies hitting resonance further out. Beyond this point, in the linear approximation, only EM waves will exist, transmitted as per the Budden approximation, Eq. (11). Figs. (10) and (11) show the progress of the initial pulse and the attendant particle acceleration. Fig. (10) graphs E_y, B_z, and n near the pulse. The pulse is still in the Alfvén mode and has not trapped many particles at $t = 200.0$ $\overline{\omega_p}^{-1}$ in Fig. (10a), and it has not quite passed the resonance region depicted in Fig. (9). In Fig. (10b), the pulse can be seen splitting (a distinctive double peak at $\xi \approx 1550$), the left half of the peak is the Alfvén mode, where $|B| > |E|$, and the right half is partly in the EM mode, where $|E| \approx |B|$. Another intriguing property here is the distinctive "wake" left by the subcyclic pulse ($1300 < \xi < 1500$ in Fig. (10b)). Fig. (11) shows the $\frac{p_\xi}{mc}$ vs ξ phase space. As the pulse propagates to the right, some particles are trapped, but not so many as in the case of the high-amplitude wavetrain, nor does the momentum increase as much, though it does become mildly relativistic. As in the previous case, a large fraction of the amplitude is transmitted, far more than predicted by the Budden approximation.

3.5. Particle Acceleration

Low intensity electromagnetic waves crossing a narrow turning point have little lasting effect on the plasma medium: the wave reaches the turning point, heats the plasma a bit at

resonance and is reflected and/or transmitted depending on the orientation of the pair of turning and resonance points. Particle acceleration enters physical consideration with large amplitudes, such that the magnetic component of the amplitude is on the order of or greater than the local background magnetic field. There are three mechanisms that can contribute to such acceleration. One possible mechanism is that of a subcyclic pulse. Rau *et al.* (1996) have shown a means by which a subcyclic (or nearly subcyclic) pulse can accelerate particles. A strong subcyclic pulse can give particles in a plasma a net acceleration in the direction of propagation, whereas a wavetrain with more than a few oscillations will not demonstrate this property. The momentum gained by the particles is

$$\gamma\beta = A \propto \int_{-\infty}^{\infty} E_y(u)du, \tag{12}$$

obtained from integrating the Lorentz equation $m_0 c\frac{d}{dt}(\gamma\vec{\beta}) = -e(\vec{E} + \beta \times \vec{B})$ where $u = x - ct$, and E_y is the y-component of the initial electromagnetic pulse. For long wavetrains, A vanishes in accordance to the Lawson-Woodward theorem (Lawson 1979; Woodward 1947), but it can be large for a subcyclic pulse. A significant property of this means of particle acceleration is that $v_e < v_{ph} = c$, where v_e is the speed of the particles. The particles are not in phase with the wave, and the resulting particle motion is ballistic. The net gain in energy is

$$\Delta\mathcal{E} \propto E_0^2, \tag{13}$$

where E_0 is the initial amplitude of the pulse at $t = 0$.

Another means of particle acceleration is via the pondermotive force (Ashour-Abdalla et al, 1981): the strong forward exertion of light pressure causes a pile up of particles in front of the light pulse. In this case, the wave is not necessarily subcyclic, but can consist of a short wave train within an envelope. The strong light pressure expels particles from where the pulse is located, both forward and back, and those expelled forward continue

to feel the pressure of the wave and are accelerated more. In the frame moving with the interface, pressure balance yields

$$2 < n >_w < p_x >_w v_g = \frac{1}{2}\frac{E_w^2 + B_w^2}{8\pi}, \tag{14}$$

where v_g is the wave-front velocity, the subscript w indicates that the fields, momentum, and density are evaluated in the moving frame (which is moving at v_g), and $< n >$ and $< p_x >$ are, respectively, the average density and momentum at the leading edge of the pulse. Also, since these particles are accelerated to relativistic speeds near c, the wave packet is Doppler shifted to a frequency below cutoff with respect to them. The Lorentz transformation into the laboratory frame yields

$$2v_g \frac{< n >_L}{\gamma_g} \frac{< p_x >_L}{\gamma_g} = \frac{1}{2}\frac{E_L^2}{\gamma_g^2} \tag{15}$$

where L indicates values as measured in the laboratory frame and $\gamma_g = \frac{1}{\sqrt{1-\frac{v_g^2}{c^2}}}$. Solving for momentum, this gives us $p_x \propto E_L^2$. In the relativistic extreme, $\gamma\beta = \frac{p_x}{mc} \gg 1$ and $\mathcal{E} = \sum_i (\gamma_i - 1)mc^2$, so both energy and momentum scale as γ, which implies that $\Delta\mathcal{E} \propto E_L^2 \propto E_0^2$ for relativistic cases, scaling similarly to the subcyclic pulse means of acceleration. The group velocity of the wave packet can be less than c, allowing the wave and the particles to travel together and accelerate over time, as opposed to the ballistic result of the previous method.

Yet a third means of acceleration, clearly demonstrated in our simulations, is acceleration by means of particle trapping in Alfvén waves (Tajima and Dawson 1980). If the initial amplitude of the wave is high enough, there is an associated trapping condition:

$$\left[\frac{kv_\parallel - (\omega - \Omega_e)}{\Omega_e}\right]^2 \leq 2\Lambda\sqrt{\Pi^2 - 1}\, sin\, \phi_0, \tag{16}$$

where $v_\parallel$ is the component of the particle velocity parallel to $\vec{k}$, $\Lambda = \frac{B_z}{B_0}$, $\Pi = \frac{(kv_\parallel - \omega)^2}{\Omega_e^2}$, and ϕ_0 is the initial angle between B_z and $v_\parallel$. If the parallel velocity of a background particle, $v_\parallel$,

satisfies this condition, the particle is trapped. There is an approximate "trapping width" associated with this condition, $v_t = \left(\frac{qE}{mk}\right)^{\frac{1}{2}}$, and the condition can be approximately written as $v_A - v_t < v_{\|} < v_A + v_t$, where $v_A \approx \frac{B_0}{\sqrt{4\pi\rho_e}}$ is the Alfvén speed. Thus, if the amplitude is extremely large, all particles are theoretically trapped (particle interaction and other nonlinear phenomena will always free some particles from trapping). This trapping occurs not only in the compressional Alfvén mode, but also the shear Alfvén mode. This model has $v_A = v_{ph} < c$, so the wave can start out slow in a high-density region and accelerate to higher velocities as it enters a low-density region. This mode of acceleration appears to be prominent in the simulations presented in this paper, insofar as the Alfvén mode region of the simulation is concerned: acceleration after mode conversion into the EM region is likely due to the two means of acceleration previously mentioned, in particular the pondermotive force for the case of the non-subcyclic pulse. For not entirely coincidental reasons, the theoretical energy gain due to this means of particle acceleration is also $\Delta\mathcal{E} \propto E_0^2$, since the rate of energy transfer to the particles is:

$$\frac{d\mathcal{E}}{dt} \propto \left(\frac{eB_z}{mc}\right)^2 \tag{17}$$

where B_z is the current amplitude of the magnetic component of the wave.

3.6. Soliton Formation

Over the long term, both nonlinear simulations (the short wavetrain and the subcyclic pulse) exhibit apparently steady-state solutions far from the hole. The trapped particles propagate self-consistently with the electromagnetic fields far into the region where the background density and magnetic field is zero (for all practical purposes). We have done a very long run (to $1500\,\overline{\omega_p}^{-1}$, in a grid of 8192 cells) to determine that the acceleration does have a limit. Simulations show that while the $\beta\gamma$ of particles increases from a maximum of

$\beta\gamma \approx 20.5$ at $t = 400.0\,\overline{\omega_p}^{-1}$ to a maximum of $\beta\gamma \approx 27.5$ at $t = 500.0\,\overline{\omega_p}^{-1}$, the increase from $t = 1400.0\,\overline{\omega_p}^{-1}$ to $t = 1500.0\,\overline{\omega_p}^{-1}$ is only from $\beta\gamma \approx 41$ to $\beta\gamma \approx 42$. This demonstrates both that the burst continues far beyond the black hole atmosphere and that the momentum of the burst has a maximum.

The case for each type of wave is shown in Figs. (12) and (13). The wavetrain in Fig. (12a) is relatively complex to the subcyclic counterpart in Fig. (12b), but there are several features in common. Each has an EM mode precursor, traveling as an ordinary "light wave", and decoupled from the trapped particles and their associated fields. As for this slower mode, the concentrations of particles are highest where the electromagnetic fields are zero, and least where the fields are highest, which implies that the pondermotive force is the primary means of acceleration. Finally, these slower modes have $|B_z| > |E_y|$, implying a kind of Alfvén wave: local density and magnetic field is high, so even though the background is essentially vacuum, this "Alfvén" wave carries its own particles and field.

There are some distinct differences between the two sets of results. The wavetrain captures several peaks of particles, which propagate mostly in tandem, but slowly spread apart from one another. The subcyclic pulse, on the other hand, captures only a single peak, with some particles that gradually fall behind, but most stay with the main peak. The phase space in Fig. (13a) for the wavetrain is much more chaotic than that of the subcyclic pulse in Fig. (13b), with particles falling in any of the several peaks, and apparently hopping from one peak to another. The subcyclic phase space, however, shows a single graceful loop, wherein particles receive an initial boost to near relativistic velocity by the EM precursor, quickly accelerate from there while gradually falling behind the main peak, then hit the rear end of the pulse (at $\xi \approx 2210$ for $t = 500.0\ \overline{\omega_p}^{-1}$) and accelerate back up to the main peak in front ($\xi \approx 2250$). These particles then slowly lose momentum until they are gradually lost behind the main body of the pulse. We suspect that the complex

behavior in Fig. (13a) is the chaotic overlapping of several modes like those in Fig. (13b).

The relative magitudes of acceleration and number of particles differs between the two simulations, but this can largely be explained by considering the dependency of the number of captured particles and their relative accelerations upon the initial amplitude of the wave. We performed four simulations at varying amplitudes in order to establish dependencies for the amount of particles trapped and the amount of acceleration produced. Similar simulations in which we merely varied the temperature of the plasma by several orders of magnitude did not appear to suggest that these quantities are dependent upon temperature. Fig. (14) shows the variation of the local number density of particles that had been accelerated and trapped (measuring the actual number is much more difficult, since the peak is narrow). These measurements were taken at the same point in time after the beginning of the simulation ($t = 500.0\,\overline{\omega_p}^{-1}$), but the actual location of the trapped particles varies, since they have been accelerated more for the large initial amplitude than for the lower amplitudes. The amount of particles trapped appears to be directly proportional to the initial amplitude of the pulse.

A graph showing the maximum gain of momentum ($\beta\gamma$) of the particles trapped is in Fig. (15). The logarithmic scale plot is very close to linear, and measurements indicate a power law relationship of about $\beta\gamma_{max} \propto {B_{z0}}^{1.26-1.66}$. Since this measures the momentum at a certain point in time in each case, as opposed to the maximum (saturated) amount of momentum after all acceleration has taken place, the power law obtained indicates a general trend rather than a physical property, and cannot be used to confirm or deny the E_0^2 law for the overall boost to the particles accelerated. The lower level of acceleration in the subcyclic case, as well as the lower number of particles trapped, appears to be entirely due to the lower effective amplitude of the subcyclic wave (which was originally set with $B_z(t = 0) = 2.5$ in code units, but a fraction of that initial energy propagated to the left of

the grid, and the actual initial amplitude is approximately $B_z(t=0) = 1.4$).

As solitons, these phenomena differ from previous theoretical models by virtue of one main characteristic: previous soliton models have a single envelope with many oscillations (Tajima and Taniuti 1990; Kaw, Sen, and Katsouleas 1992). In our case, especially in the subcyclic simulation, a solitary pulse is by itself the wave oscillation (i.e., ours is not an envelope soliton).

4. Photon Spectra and Applications to Black Hole Outbursts

Via means discussed in Section 3, we can postulate particles accelerated from nearby a black hole to distances several R_s away and beyond. Linear arguments indicate that most such energy would be absorbed, and very little energy would escape the region near the event horizon, but our nonlinear simulation shows that a violent outburst is very capable of capturing particles (via Alfvén mode wave trapping near the horizon), and accelerating them to the theoretical resonance point, beyond which the pondermotive force takes over and accelerates them to a saturation energy level far from the hole.

We plot photon energy spectra converted from electrons generated by the two main simulations in Figs. (16) for the wave packet and the subcyclic pulse, at $t = 500.0\ \overline{\omega_p}^{-1}$. The photon spectrum is calculated based on the bremsstrahlung from accelerated electrons as

$$\mathcal{G}(\epsilon) = N_0 \frac{mc^2}{\epsilon} \int_\epsilon^\infty \frac{1}{(1 + E_k/mc^2)^3} f(E_k) dE_k, \tag{18}$$

where E_k is the kinetic energy of the electrons, and $f(E_k)$ is the kinetic energy distribution of the electrons obtained from our simulations. This formula was obtained by changing from velocity to kinetic energy in the standard expression, and is approximately valid for both

nonrelativistic and relativistic regimes, as long as the particles are not ultrarelativistic. N_0 is an arbitrary normalization factor. Both photon spectra in Fig. (16) have a "knee" where the power law changes slightly, both at about $10^{3.2}$ keV more sharply defined. The slope of the low energy (< 1MeV) range is about -1, though it gets harder for the very low energies. After the knee, the slope decreases very sharply (about -6).[1] In these observations, the low-energy slopes vary from -1 to -1.3, and the slopes at high energy vary from -4 to -6 or higher, and the position of the knee varies from $10^{2.9}$ to $10^{3.8}$ keV. The typical high energy slopes should range from -2 to -4 (Pelaez et al. 1994), but Comptonization rather than bremsstrahlung is likely the responsible process here. (In our work, Comptonization is not incorporated yet.) The "lump" at about 10^2 keV in Fig. (16b) comes from the reflected pulse that was inadvertently generated. It accelerates particles much as the main pulse does, but since it has not accelerated them very much yet, it appears at a lower energy. In the wavetrain spectrum, a similar phenomenon occurs (several distinct wavefronts, each at a different energy level), but it is less distinct since the energies are relatively close together.

5. Conclusion

We have employed a conformalism for general relativistic plasma physics that greatly simplifies the dynamical study in a strong Schwarzschild background and a simulation model based on this formalism, which has enabled us to simulate a possible mechanism for outbursts from a black hole atmosphere. Bursts as we conceive them can be caused by at least two possible mechanisms. The obvious mechanism is that there is an accretion

[1]This is qualitatively consistent with observed spectra of bursty X-rays and γ-rays which in many cases have multiple power laws (Nolan et al 1984; Harding, Pe, and Teegarden 1986).

disk, which could spew out matter through some instability towards the event horizon. This can excite an Alfvén wave similar to those we have modelled, capable of accelerating the precipitated matter away from the hole. A prime application of this type of model would be the black hole candidate GRO J1655-40, which shows evidence of an accretion disk and displays bursty behavior of the type we discuss. A second mechanism would be given a moderately stable black hole "atmosphere" within $3R_s$, as discussed in Tarkenton (1996), numerous instabilities are possible (since there is no "bottom" to the atmosphere) which can excite Alfvén modes near the event horizon and accelerate particles in a manner similar to that which we have modelled. These specific examples should not be construed as the only two possibilities: a wide variety of possible initial conditions involving an event horizon may conceivably excite Alfvén waves as described and modelled in this paper, and the model can be scaled to a stellar mass black hole or to an AGN. We have shown that internal magnetic modes can be converted not only into external electromagnetic emissions, but can trap and accelerate particles to relativistic velocities. Furthermore, we have shown that the mode conversion for high amplitude waves occurs much more efficiently when linear WKB analysis no longer applies and the self-induced transmission phenomenon arises. This means that the strong near-horizon magnetic disturbance has a much greater transmission percentage into the upper atmosphere than the linear theory prediction and thus may provide a scenario for a realistic strong wave excitation associated with a outburst episode. This anomalously efficient mode conversion into EM waves combined with the above efficient acceleration of electrons presents an excellent candidate for the source of energetic electrons for bursty episodes.

Photon spectra of the emissions from electrons accelerated by this process away from the horizon are simulated which are qualitatively consistent with previously observed bursty phenomena. This is a 1-d simulation, however, and results in two or three dimensions can

be important. A new means of examining phenomena arising from a plasma in a strong gravitational field has been provided that allows us to adopt the techniques developed in "flat" plasmas to this new regime of plasma wave behavior. The general relativistic plasma physics begins to offer some observable signatures in electromagnetic waves (optical and X-rays and γ-rays) near a black hole horizon.

Work was supported in part by US DoE and NSF.

REFERENCES

Ashour-Abdalla, M. et al, 1981, Phys. Rev. A, 23, 1906

Balbus, S., and Hawley, J., 1991, ApJ, 376, 214

Blaes, O. M., 1987, MNRAS, 227, 975

Budden, K. G., 1961, Radio Waves in the Ionosphere (Cambridge: Cambridge University Press)

Buzzi, V., Hines, K. C., and Treumann, R. A., 1995, Phys. Rev. D, 51, 6663

Daniel, J., and Tajima, T., 1997, Phys. Rev. D, 55, 5193

Futterman, J. A. H., Handler, F. A., and Matzner, R. A., 1988, Scattering from Black Holes (Cambridge: Cambridge University Press)

Harding, A. K., Petrosian, V., and Teegarden, B. J., 1986, AIP Conf. Proc. 141, Gamma Ray Bursts, ed. E. P. Lang and V. Petrosian (New York: AIP)

Holcomb, K., and Tajima, T., 1989, Phys. Rev. D, 40, 3809

Holcomb, K., and Tajima, T., 1991, ApJ, 378, 682

Kaw, P. K., Sen, A., and Katsouleas, T., 1991, Phys. Rev. Lett., 68, 3172

Lawson, J. D., 1979, IEEE Trans. Nucl. Sc. NS-26, 4217

MacDonald, D., and Thorne, K., 1982, MNRAS 198, 345

McCall, S. L., and Hahn, E. L., 1969, Phys. Rev. 183, 457

Misner, C., Thorne, K., and Wheeler, J., 1973, Gravitation (New York: W. H. Freeman and Company)

Mobarry, C. M., and Lovelace, R. V. E., 1986, ApJ, 309, 455

Murakami, T., 1988, in "Physics of Neutron Stars and Black Holes", ed. Y. Tanaka (Tokyo: Universal Academy) p. 605

Nolan, P. L., et al, 1984, AIP Conf. Proc. 115, High Energy Transients in Astrophysics, ed. S. E. Woosley (New York: AIP)

Orosz, J. R., et al, 1997, ApJ, 478, L83

Pelaez, et al, 1994, ApJS, 92, 651

Rau, B., Tajima, T., and Hojo, H., 1996, Phys. Rev. Lett. 78, 3310

Tajima, T., and Lee, Y. C., 1981, J. Com. Phys. 42, 406

Tajima, T., and Dawson, J. M., 1980, Nuclear Fusion, 20, 1129

Tajima, T., 1989, Computational Plasma Physics (Reading, MA: Addison-Wessley)

Tajima, T., and Tanuiti, T., 1990, Phys. Rev. A, 42, 3587

Tanaka, Y., 1989, in Proceedings of the 23rd ESLAB Symposium — X-ray Astronomy, edited by J. B. Battrick et al (Paris: ESA, SP-296), p. 3

Tarkenton, G., 1996, Ph.D. Dissertation at University of Texas, Austin

Thorne, K. S., Price, R. H., and MacDonald, D. A.,, 1986, Black Holes: The Membrane Paradigm (New Haver: Yale University Press)

Woodward, P. M., 1947, Journal IEE, 93, Part IIIA, 1554

This manuscript was prepared with the AAS LaTeX macros v4.0.

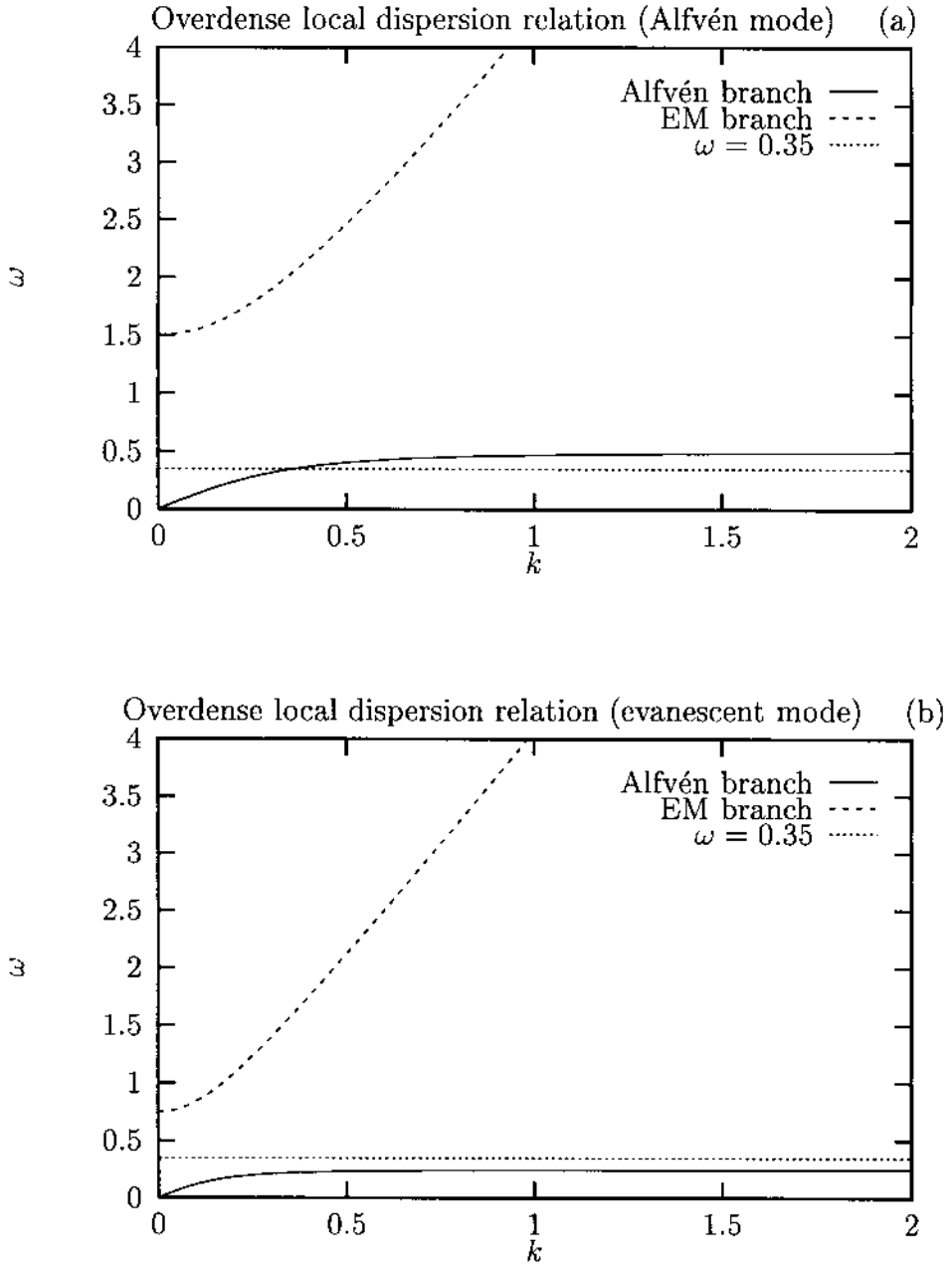

Fig. 1.— An overdense plasma inhibits mode conversion, since there is a large difference between the resonant and cutoff frequencies. The intermediate region, where $\omega(k)$ has no real value for either branch, is evanescent: waves of these frequencies decay exponentially. Plot (a) shows a wave of frequency $\omega = 0.35$ in a region of Alfvén propagation, and (b) shows a wave of the same frequency in the evanescent region at a later point in space and time.

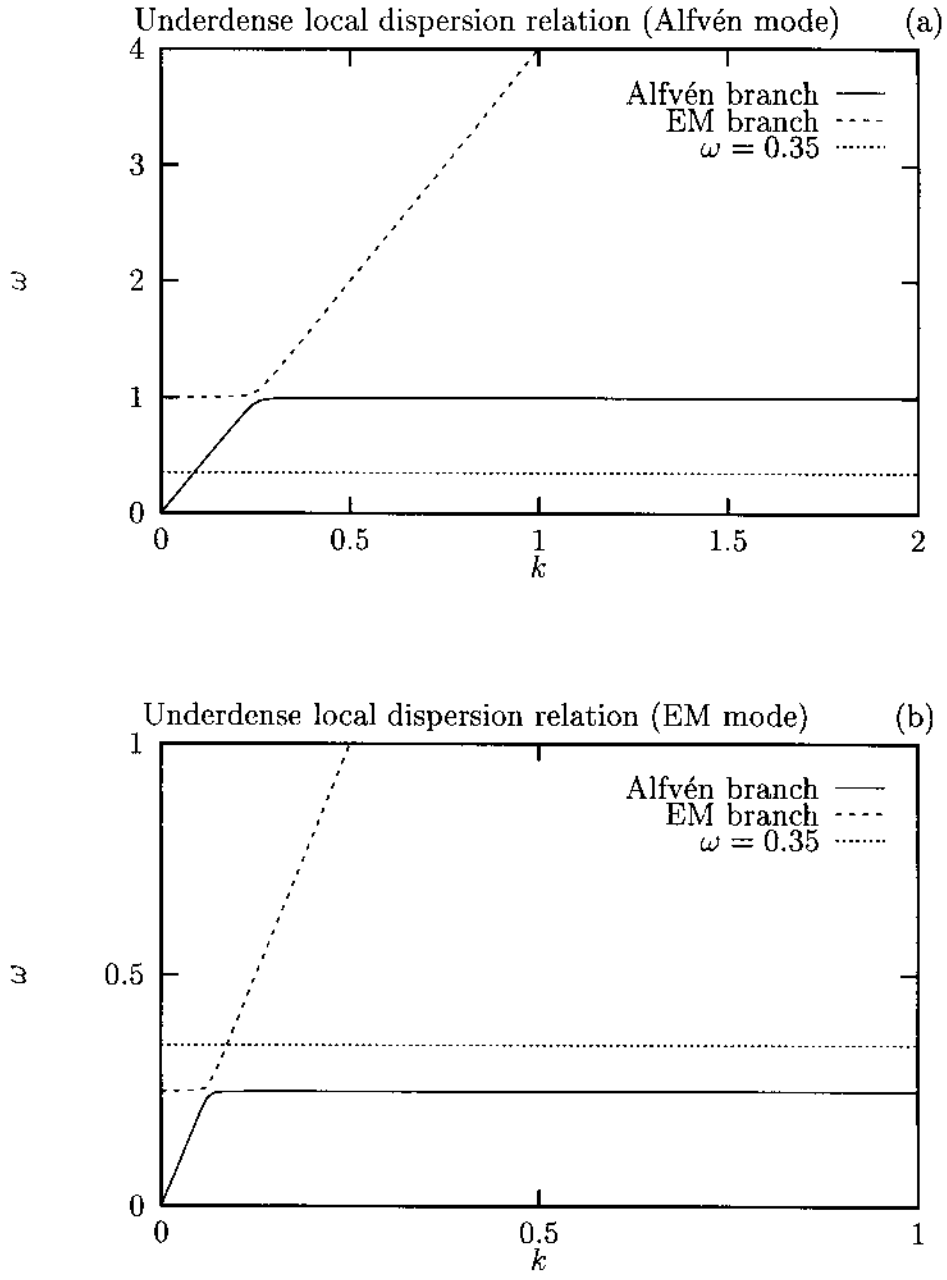

Fig. 2.— An underdense plasma facilitates mode conversion, since the region between the cutoff and resonant frequencies is small. Graph (a) shows a sample Alfvén case where the given frequency lies in the Alfvén branch, and (b) shows the same frequency at a later point in time and space, now in the EM branch. Note how the two branches almost touch in the underdense case, allowing for efficient mode conversion.

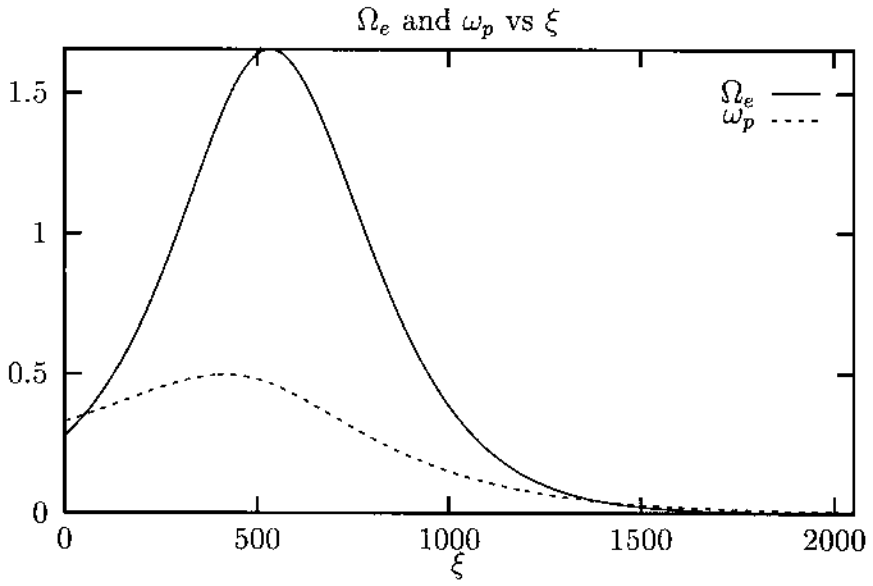

Fig. 3.— The typical conformalized background cyclotron frequency $\Omega_e(\xi)$ and plasma frequency $\omega_p(\xi)$ profiles for the simulations to be discussed.

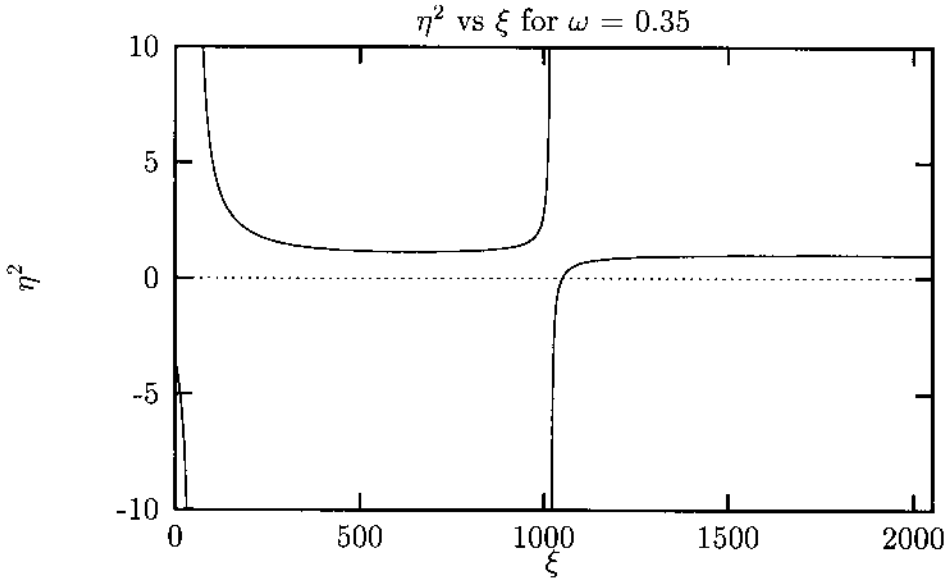

Fig. 4.— This plots η^2 (the index of refraction) vs ξ, for the primary frequency of the wave packet discussed in Section 3.2. There is a turning point at $\xi \approx 1020$ (where a resonance occurs) to $\xi \approx 1050$ where there is a cutoff.

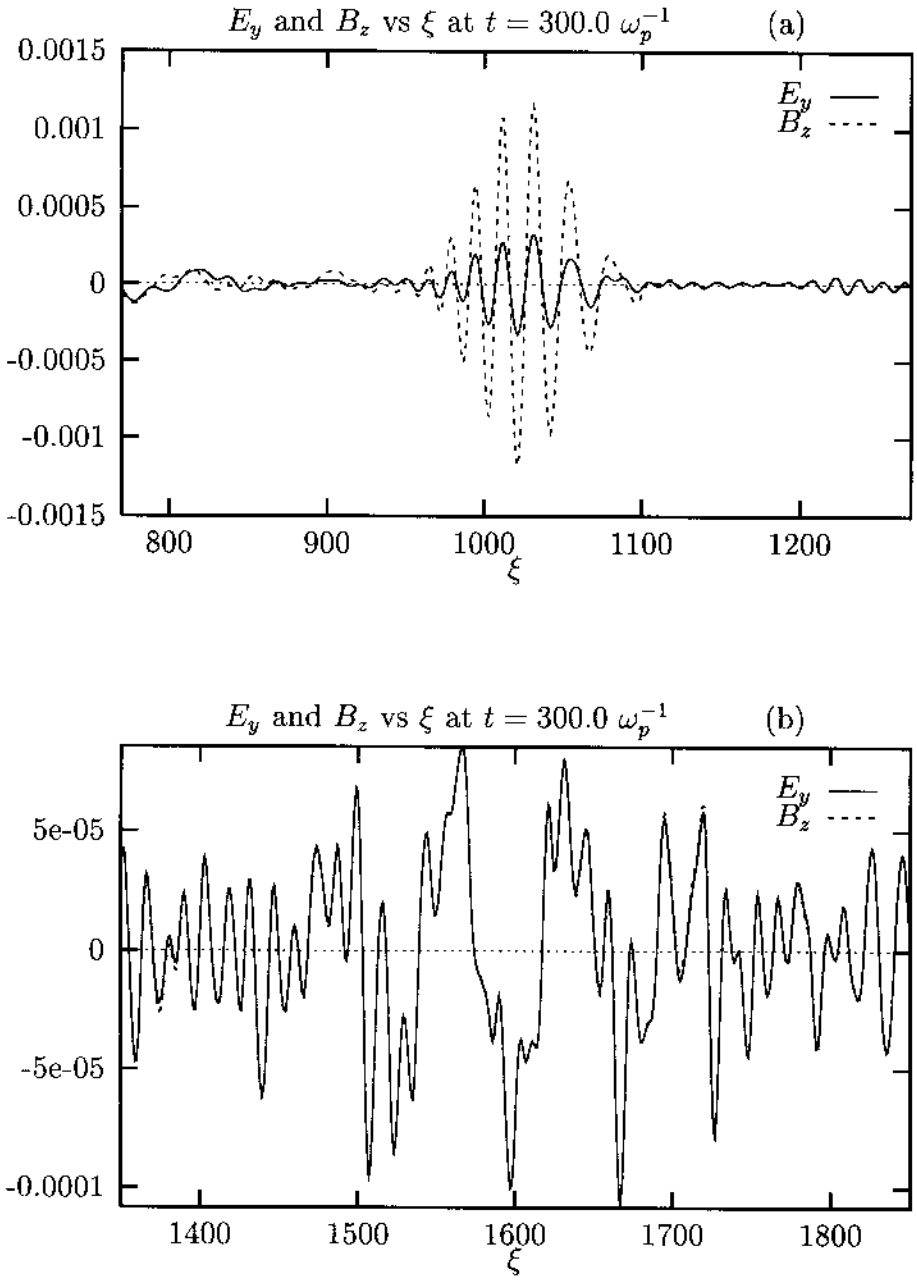

Fig. 5.— Electric and magnetic fields in ξ-space for a low-amplitude wave going through mode-conversion. The wave has reached resonance in (a), and some has been transmitted in EM mode in (b) at $\xi \approx 1600$.

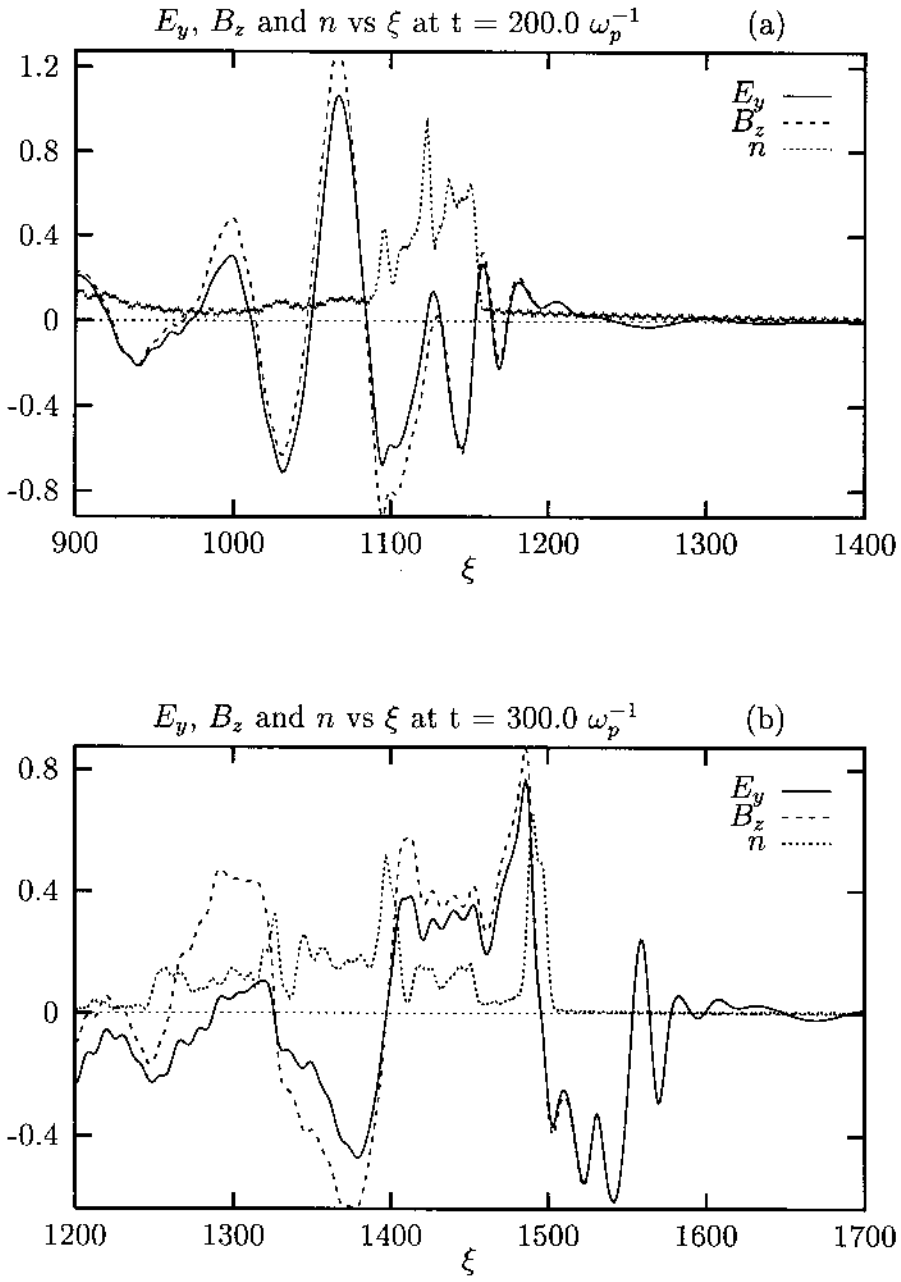

Fig. 6.— Electric and magnetic fields plotted along with local number density n. In (a), mode conversion has already occurred ($\xi > 1050$), and the a large number of particles have been carried out from the atmosphere, where (b) the wave packet spreads out into several modes, including a precursor (with $E_y = B_z$, to the right) and what is apparently a type of soliton.

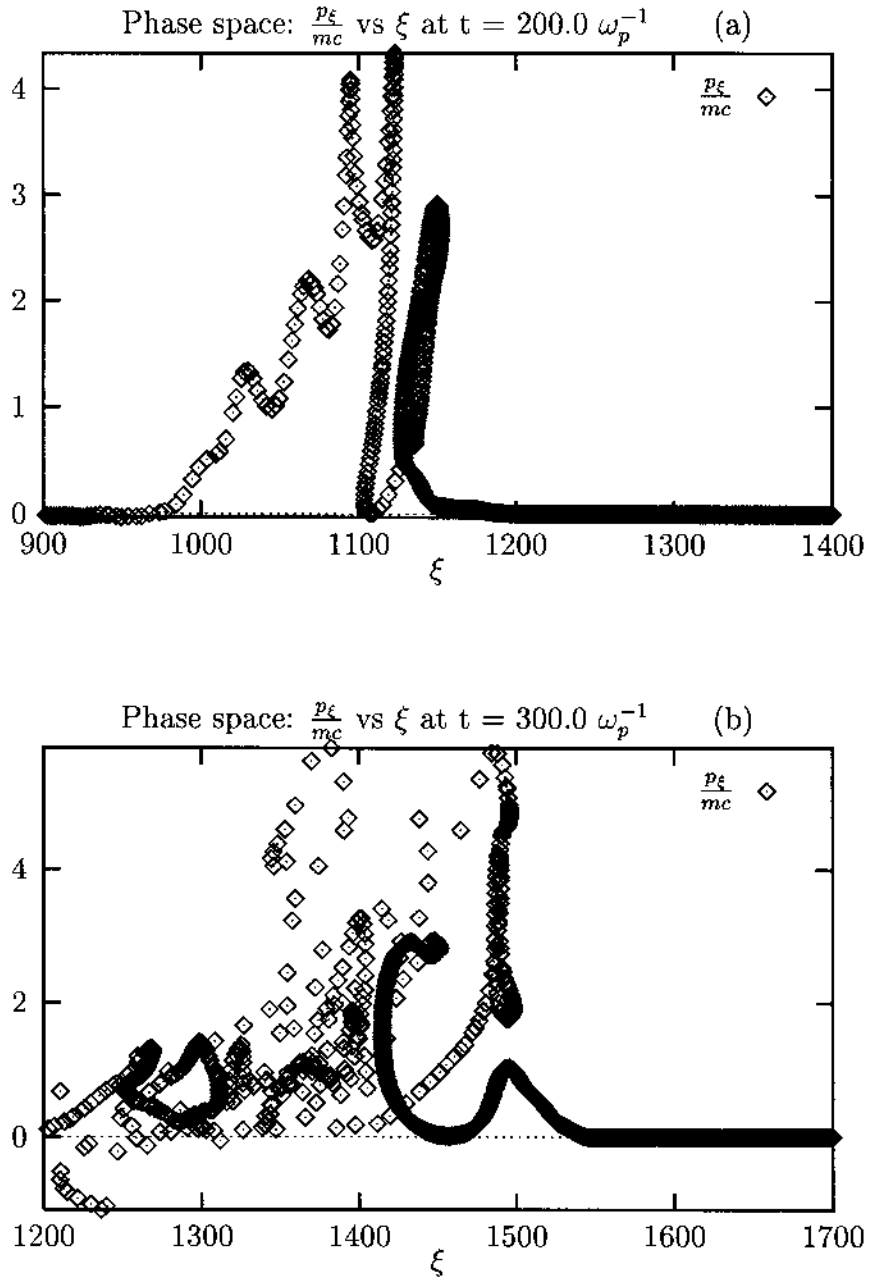

Fig. 7.— Phase space of the particles near the wave packet. Particles are clearly trapped in (a), and continue to be trapped and accelerated beyond the nominally Alfvén region.

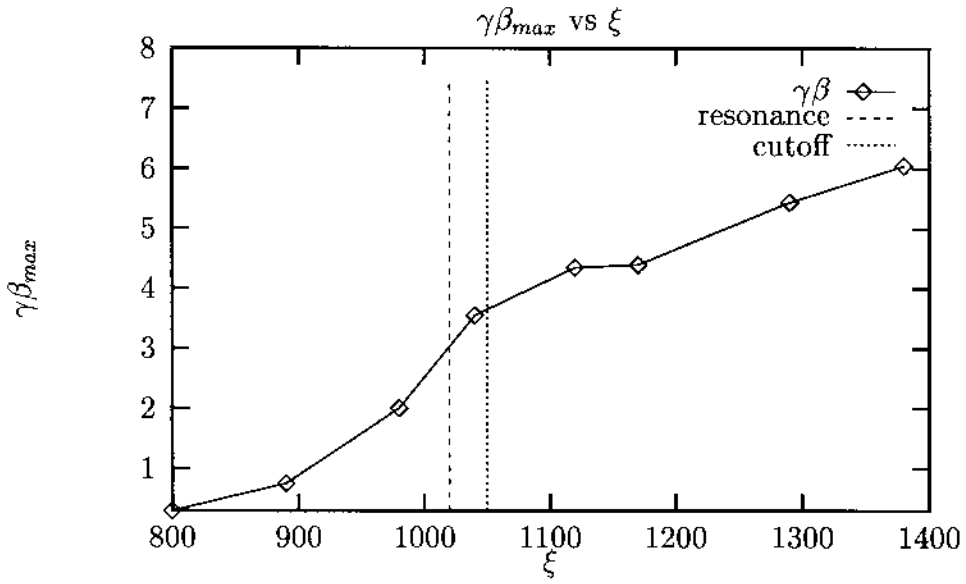

Fig. 8.— This is a parametric plot of $\gamma\beta_{max}$ vs ξ at even time intervals (every 25.0 $\overline{\omega_p}^{-1}$) as particles are accelerated to relativistic velocities ($\gamma\beta > 1.0$). The rate of acceleration increases geometrically in the Alfvén region ($\xi < 1020$), to reach relativistic velocities as it approaches resonance. After resonance and mode conversion into the EM wave region, the acceleration slows until $\xi = 1170$, well past the turning point.

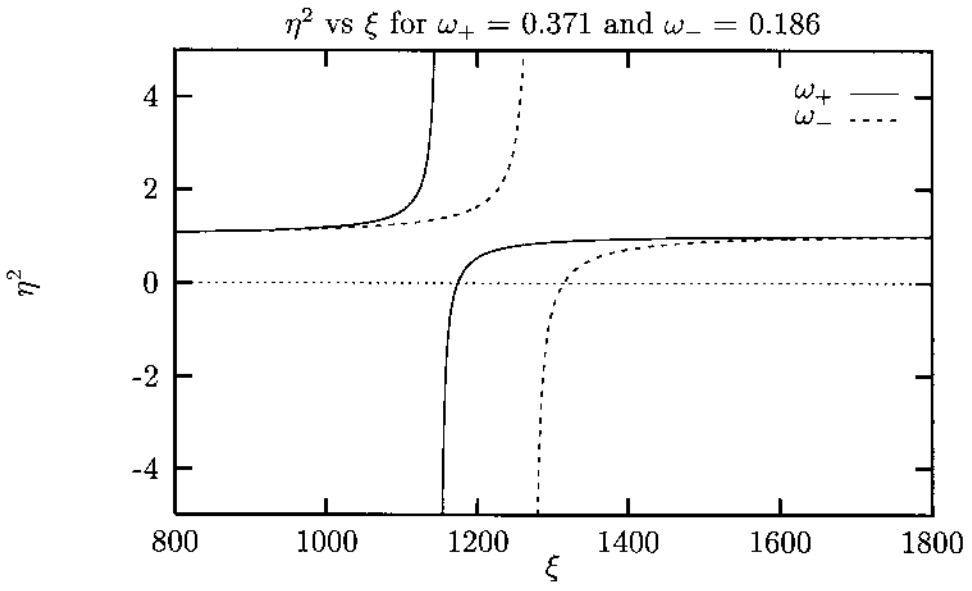

Fig. 9.— We plot η^2 (the index of refraction) vs ξ for a range of values of ω, which represent the range of frequencies found in the solitary wave. The two turning points shown represent the range over which resonance will occur for most of the wave.

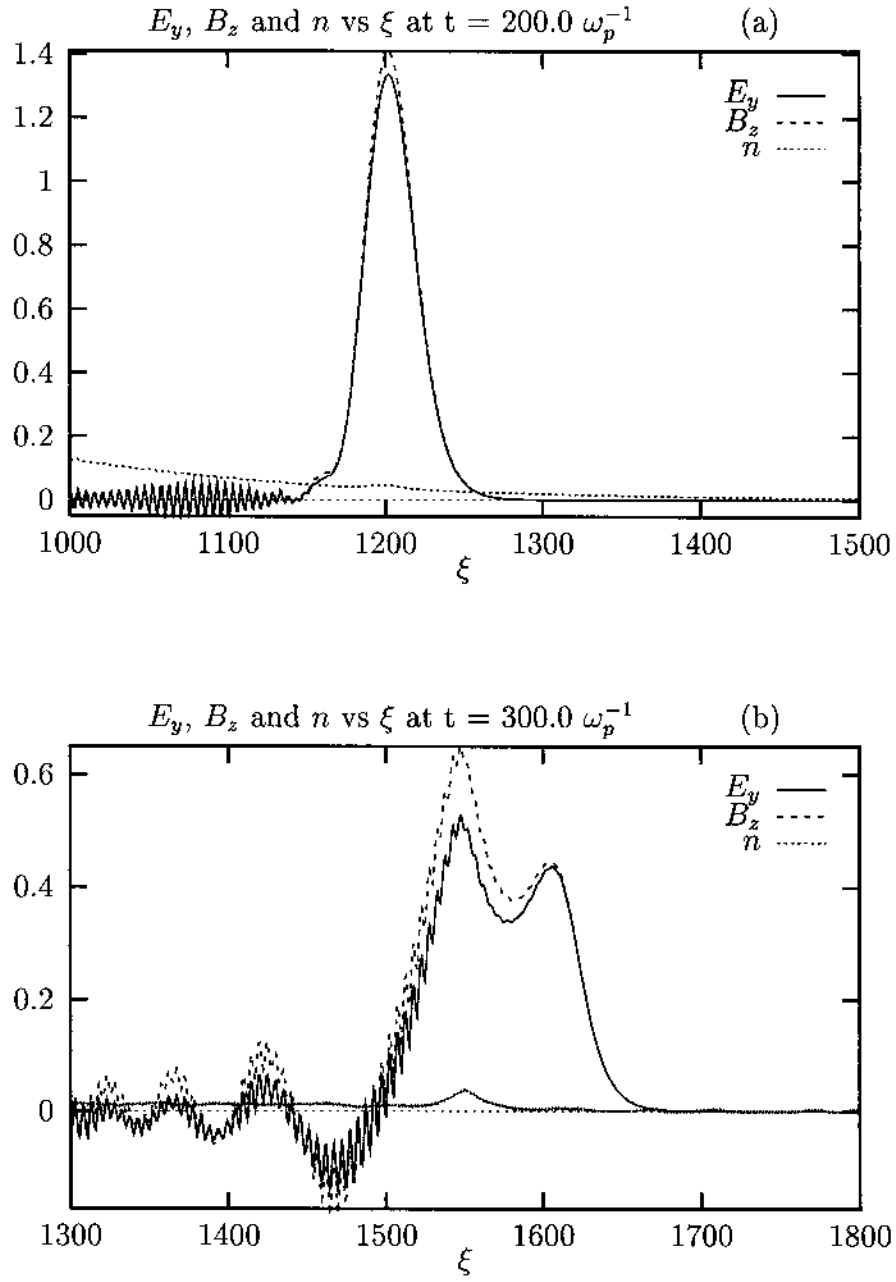

Fig. 10.— The transverse electromagnetic field (E_y and B_z) of a solitary wave (initial amplitude = 2.5 in code units). It propagates from the left to the right, exhibiting mode conversion in (b), where there is a distinctive double peak at $\xi \approx 1600$: the left peak is still in the Alfvén mode of the original pulse, and the right peak is approaching the electromagnetic mode.

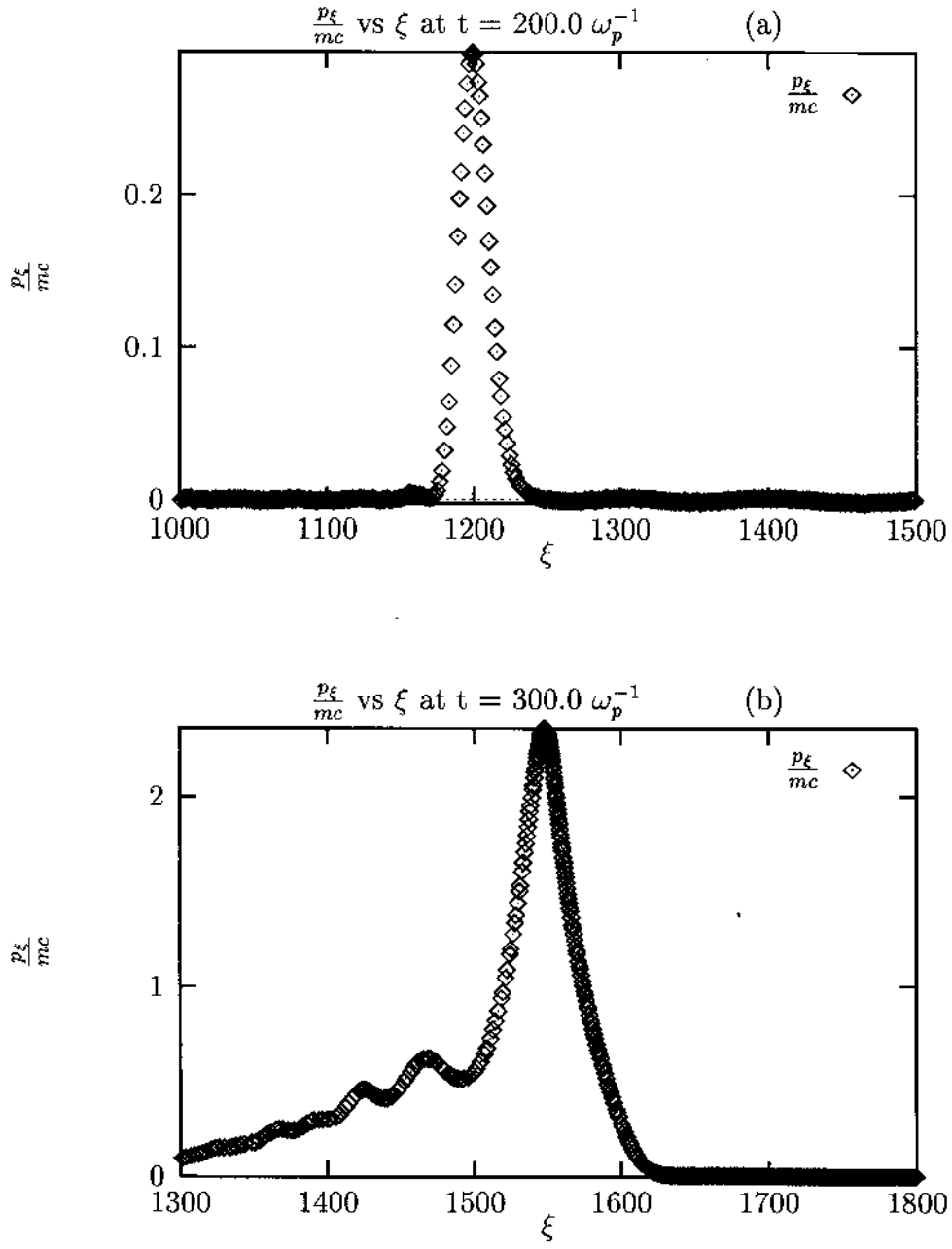

Fig. 11.— $\frac{p_\xi}{mc}$ $(=\beta\gamma)$ vs ξ phase space. Positrons and electrons of the plasma are accelerated to relativistic velocities. Note that particles are not trapped as in the the short wavetrain (see Fig. (7), and arent accelerated to high velocities as quickly.

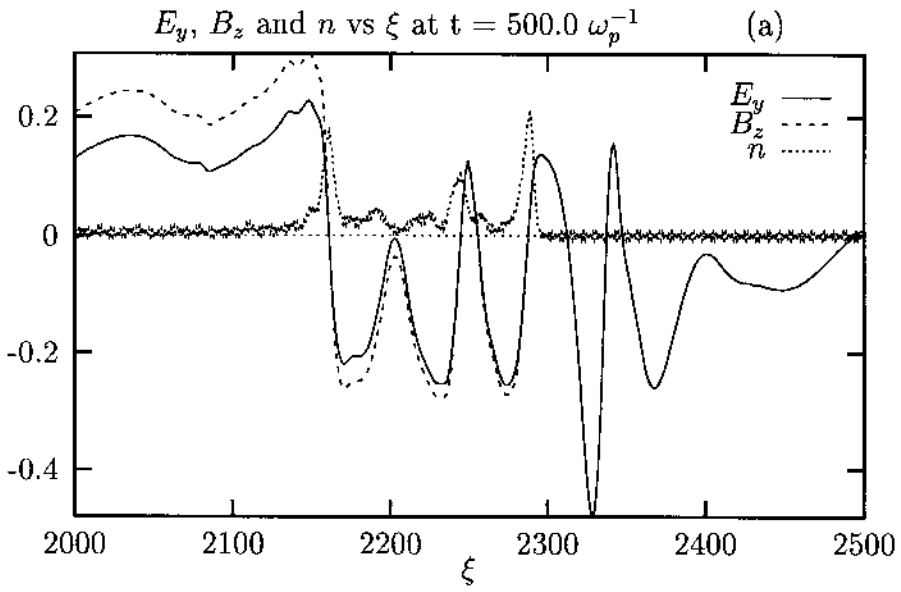

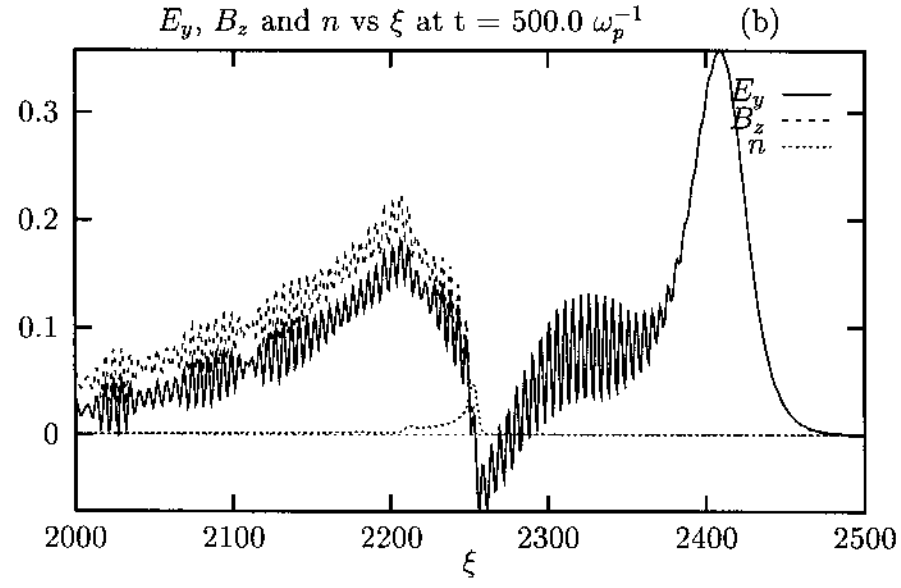

Fig. 12.— The electromagnetic fields and densities late in the runs (at t = 500.0 $\overline{\omega_p}^{-1}$) for the wave packet (a) and the subcyclic pulse (b).

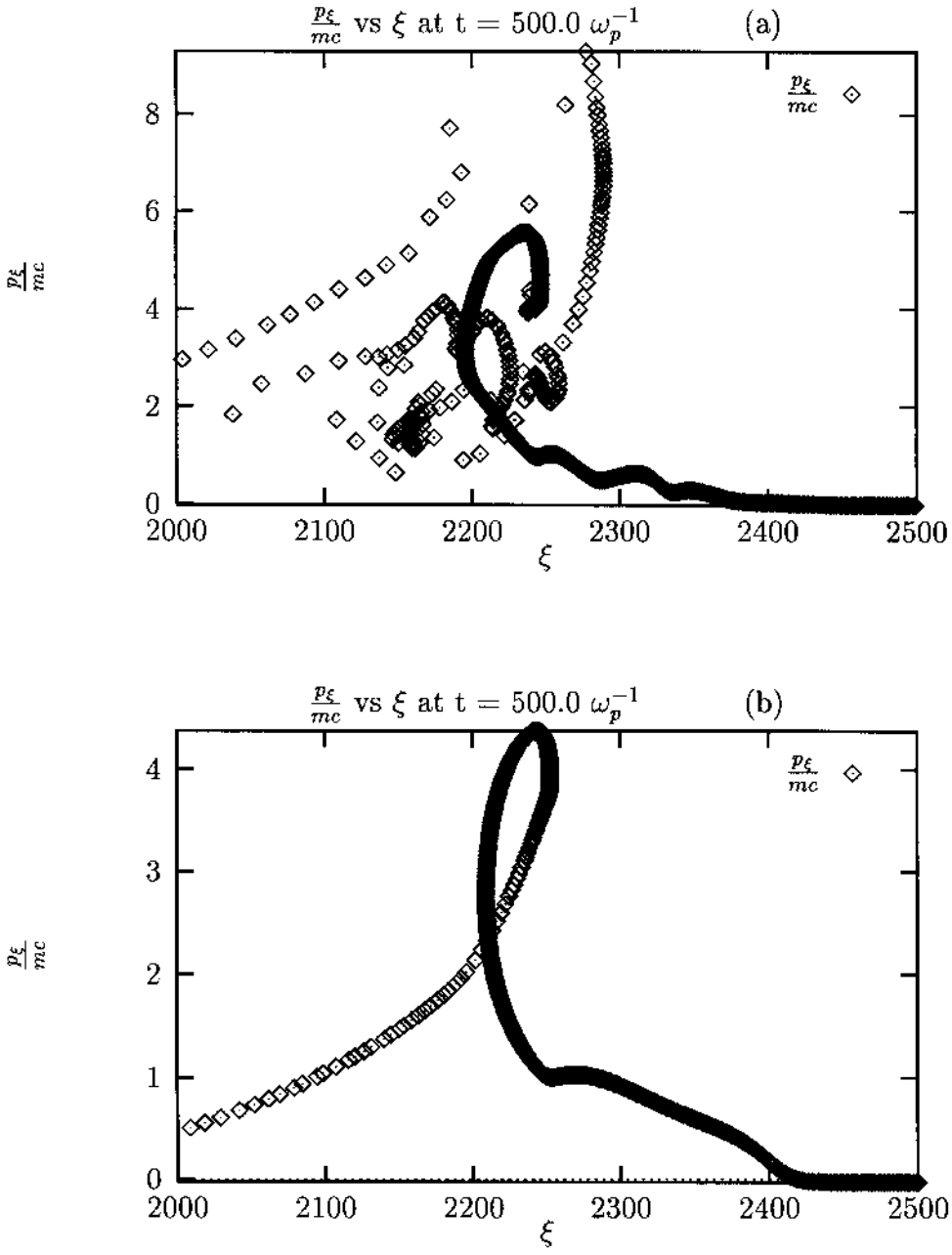

Fig. 13.— The $\frac{p_\xi}{mc}$ $(=\beta\gamma)$ vs ξ phase space for the wave packet (a), and the subcyclic pulse (b).

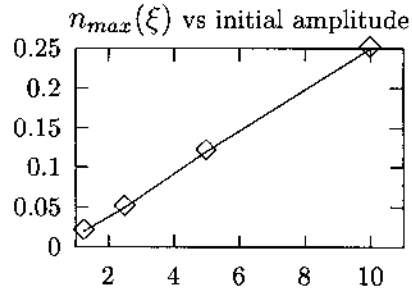

Fig. 14.— Maximum number density vs initial amplitude of trapped particles at $t = 500.0\overline{\omega_p}^{-1}$, which is a rough measure of the total number of particles trapped. (The number density is fractional since the density is a weighted quantity.)

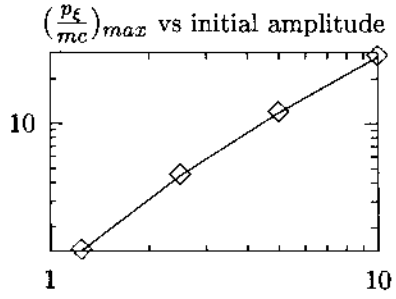

Fig. 15.— The quantity $\frac{P_\xi}{mc} = \beta\gamma$ is graphed here as a function of initial amplitude. It is a measure of the maximum magnitude of momentum imparted to the particles after $500\overline{\omega_p}^{-1}$ as a function of initial amplitude of the solitary pulse. The initial amplitude was doubled for each successive measurement from 1.25 to 10.0 (as measure in code units).

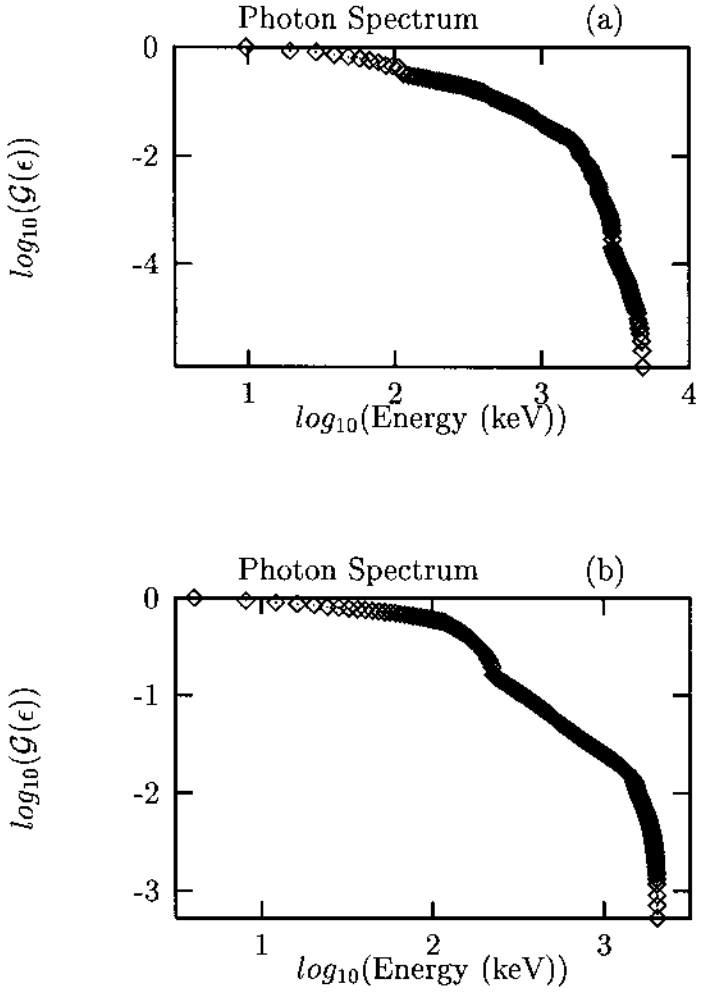

Fig. 16.— Photon spectra for the wave packet simulation (a) and the solitary wave simulation (b) run (at t = 500.0 $\overline{\omega_p}^{-1}$).